Solar Energy Materials & Solar Cells 160 (2017) 410–417

Contents lists available at ScienceDirect

Solar Energy Materials & Solar Cells

journal homepage: www.elsevier.com/locate/solmat

Influence of silicon on high-temperature (600 °C) chlorosilane interactions with iron

Josh Aller[a,*], Nolan Swain[b], Michael Baber[a], Greg Tatar[b], Nathan Jacobson[c], Paul Gannon[b]

[a] Mechanical and Industrial Engineering, Montana State University, Bozeman, MT 59717, USA
[b] Chemical and Biological Engineering, Montana State University, Bozeman, MT 59717, USA
[c] NASA Glenn Research Center, Cleveland, OH 44135, USA

ARTICLE INFO

Keywords:
Iron
Chlorosilane
Silicon
Silicon tetrachloride
Iron silicide
Corrosion

ABSTRACT

High-temperature (> 500 °C) chlorosilane gas streams are prevalent in the manufacture of polycrystalline silicon, the feedstock for silicon-based solar panels and electronics. This study investigated the influence of metallurgical grade silicon on the corrosion behavior of pure iron in these types of environments. The experiment included exposing pure iron samples at 600 °C to a silicon tetrachloride/hydrogen input gas mixture with and without embedding the samples in silicon. The samples in a packed bed of silicon had significantly higher mass gains compared to samples not in a packed bed. Comparison to diffusion studies suggest that the increase in mass gain of embedded samples is due to a higher silicon activity from the gas phase reaction with silicon. The experimental results were supported by chemical equilibrium calculations which showed that more-active trichlorosilane and dichlorosilane species are formed from silicon tetrachloride in silicon packed bed conditions.

1. Introduction

Chlorosilane species are used at high temperatures in the refinement, manufacture, and deposition of silicon and silicon-containing species [1–4]. They include many hydrogen, silicon, and/or chlorine containing compounds including silicon tetrachloride ($SiCl_4$, STC), trichlorosilane ($HSiCl_3$, TCS), dichlorosilane (H_2SiCl_2, DCS), and silane (SiH_4). Often times they are combined with hydrogen (H_2) as a carrier gas and hydrogen chloride (HCl) from various processing steps [1–4]. At high temperatures, high cost nickel based alloys are generally employed to handle these species due to their corrosion resistance. However, these high cost alloys greatly contribute to the overall cost of the final silicon or silicon containing product [5,6]. This is certainly the case in the manufacture of solar silicon feedstock; the most prevalent application of chlorosilanes at high temperatures. Iron, a primary component of low cost alloys, will be the primary focus of this study.

Like many gas mixtures, the composition of a chlorosilane mixture changes dramatically when it is heated from room temperature to high temperatures seen in industry (approximately 600 °C). For example, a STC/H_2 input stream may form significant amounts of TCS, DCS, and HCl when it is heated [1,4–9]. The presence of materials that can vaporize into the gas stream further complicates these reactions. The most common material added to a chlorosilane gas stream is silicon. Silicon may be present in a fluidized bed reactor used to convert silicon tetrachloride to trichlorosilane or deposition equipment used to deposit silicon on a wafer. In each case, the reactor's material of construction must be able to withstand the new environment created by the STC/H_2/Si mixture at high temperatures.

Previous investigations have been performed to study the corrosion behavior of various metals and alloys in high temperature chlorosilane environments. The presence of both silicon and chlorine in chlorosilanes creates a complex corrosion environment due to the ability of many metals to form both chlorides and silicides. In the case of iron, silicide species are generally condensed [7,10,11] while chloride species are volatile [12,13] at the applicable temperatures. A significant amount of work has been reported on the chemical vapor deposition of silicon onto iron. Rebhan et al. found that iron exposed to a silane environment resulted in a Fe_3Si layer when the deposition took place at less than 600 °C [14,15]. After silane exposures above 800 °C, the result was primarily silicon diffused in to an iron substrate without forming a new compound. Klam et al. investigated the influence of silicon source on the chemical vapor deposition of silicon on iron at high temperature (750–1100 °C) [16]. This study found that with an STC source, there was a significant amount of porosity in the Fe_3Si

Abbreviations: $SiCl_4$, STC, Silicon Tetrachloride; $HSiCl_3$, TCS, Trichlorosilane; H_2SiCl_2, DCS, Dichlorosilane; MG-Si, Metallurgical Grade Silicon; FEM, Field Emission Scanning Electron Microscope; EDS, Energy Dispersive X-Ray Spectroscopy; XRD, X-Ray Diffraction

* Correspondence to: Montana State University, 306 Cobleigh Hall, Bozeman, MT 59717, USA.
E-mail address: Josh.aller@yahoo.com (J. Aller).

http://dx.doi.org/10.1016/j.solmat.2016.11.002
Received 20 September 2016; Received in revised form 25 October 2016; Accepted 2 November 2016
Available online 12 November 2016

layer that was not seen with a silane source. This porosity was attributed to the formation of volatile chlorides that vaporized from the sample, leaving porous voids behind. Acker has published on the behavior of metals in chlorosilane environments with a focus on making metal silicides and catalyzing the conversion of STC to TCS [17–19]. His work laid the framework for understanding how metal silicides form and behave in chlorosilane environments, but it was not focused on the corrosion behavior of the metal. The authors have previously reported on the corrosion behavior of AISI 316L and pure iron in an input stream of STC and H_2 and found that silicide and chloride formation depends on the time, temperature, and amount of HCl in the exposure [20–23]. Iron samples above 600 °C formed stratified FeSi and Fe_3Si layers with a significant amount of porosity from chloride formation. AISI 316L corroded significantly less than iron in similar conditions likely due to the additional alloying elements. Although this work was conclusive, it did not look at the effect of changing the chlorosilane composition.

Mui investigated the behavior of a wide variety of metals in a packed bed of silicon that were exposed to a STC/H_2 input stream and found that they largely formed a silicide layer [7]. He was primarily performing a materials screening experiment to decide which materials were best for constructing chlorosilane handling equipment. While his work served this purpose, the complexities associated with highly alloyed metals did not allow him to make fundamental claims about the corrosion phenomena in a chlorosilane environment with a packed bed of silicon. There have been additional studies looking at the interaction of solid iron with solid silicon at high temperatures in inert environments. These studies are important to understand to account for the solid-solid interaction of silicon and iron. Baldwin and Ivey studied the iron-silicon diffusion couple at 700–800 °C for times up to several months and found Fe_3Si formed first, followed by FeSi, and $FeSi_2$ [24]. There was near negligible compositional variation within the layers contrary to the iron-silicon phase diagram which predicts a range of variability. Zhang and Ivey were able to form non-stoichiometric $Fe_{3+x}Si_{1-x}$ using a Fe_3Si–Fe diffusion couple [25]. However, it grew very slowly compared to stoichiometric Fe_3Si, so its formation is not predicted to be as common.

A thorough literature review has revealed that while there is a significant amount known about the interaction of iron and chlorosilane species, there are still some fundamental questions that need to be answered. This study focuses on the influence of solid silicon on the corrosion behavior of pure iron with an input stream of H_2 and STC. This setup very closely imitates industrial environments in a way that has not been reported previously. Understanding what influence solid silicon has on corrosion behavior will allow users to effectively design cost efficient alloys for use in industries that use chlorosilanes, including the manufacture and refinement of solar grade silicon.

2. Experimental setup

In previous work, the authors described the methods and provided diagrams of the test apparatus for exposing metals to an adjustable chlorosilane environment [20]. However, for clarity it will be again described here. 50 sccm of hydrogen gas was bubbled into the bottom of a 1 l bottle containing liquid STC. As the hydrogen bubbles rose through the STC, they became fully saturated with STC making the head space a mixture of hydrogen gas saturated with STC vapor. This mixture flowed out of the outlet of the bottle where it was combined with a make-up stream of 10 sccm of hydrogen. The mixture then flowed into the quartz tube furnace, across the samples, and to a scrubbing system. The amount of STC added to the hydrogen line was measured each run by taking the mass of the STC bottle before and after. The total input stream was generally a 0.74 mol fraction of H_2 and 0.26 mol fraction of STC. A total flow rate of approximately 80 sccm combined with a tube furnace diameter of 26.8 mm lead to a bulk gas velocity of 14 cm/min. Experiments were run for a variety of times less than 100 h at a temperature of 600 °C.

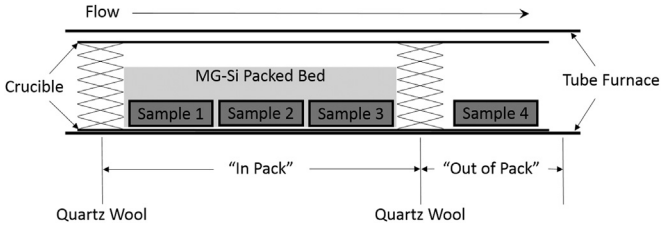

Fig. 1. Cross sectional diagram showing the layout of the tube furnace used for chlorosilane exposure and the terminology used to describe the location of samples.

The primary difference in this work compared to previous work was the addition of granular metallurgical grade silicon (MG-Si) to the tubular crucible. Fig. 1 shows the general layout of the inside of the tube furnace with the additional MG-Si surrounding the first three samples and held in place by loosely packed quartz wool that allowed gas to flow through it. These samples are referred to as “in pack”. One “out of pack” sample was placed immediately after the quartz wool downstream of the MG-Si. Only one sample was used here due to space constraints. Samples run in previously reported exposures without any MG-Si present are referred to as “no pack”. Additionally, some runs were performed with samples “in pack” with a 5% hydrogen 95% argon mixture. The purpose of these runs in a reducing environment were to study the effect of pure silicon diffusion into the iron. These runs will be referred to as "reducing diffusion".

The iron used in this experiment was 99.6% pure with weight percent impurities of 0.025 carbon, 0.03 chromium, 0.04 copper, 0.18 manganese, 0.05 nickel, 0.012 phosphorous, 0.025 sulfur, and 0.05 silicon. Samples were cut to approximately 12 mm×12 mm×1.5 mm, deburred, and rinsed with isopropanol and water. Sample surfaces had a 1200 grit finish prior to exposure. The MG-Si had an approximate average particle size of 100–400 μm prior to exposure. Energy dispersive X-ray spectroscopy was performed on the MG-Si as received, and no impurities were detected. However, it is very likely that there are many impurities present that were below the detectable limits of EDS without standards. Common impurities in MG-Si are iron, copper, nickel, arsenic, aluminum, phosphorous, and boron. These impurities are also known to catalyze the STC to TCS conversion reaction [1,9].

Surface analyses, cross sectional analyses, and gravimetric analyses were all employed in this experiment. Ex-situ gravimetric analysis included a Sartorius microbalance with 2 microgram precision. As is common for this type of work, mass change was normalized by dividing by sample surface area to make the results geometrically independent. Time-dependent mass results were compared to idealized parabolic kinetics by plotting specific mass change against the square root of time. For purely diffusion limited, parabolic behavior, this will result in a straight line going through zero with the slope of that line equaling the square root of the parabolic rate constant. If the data deviates from this line, it signifies non-parabolic kinetics. Surface analysis included the use of a Zeiss Supra 55VP field emission scanning electron microscope (FEM), energy dispersive X-ray spectroscopy (EDS), and a Scintag X1 X-ray diffraction (XRD) system and Jade software for pattern analysis. EDS was used without standards, so atomic concentrations were interpreted qualitatively rather than quantitatively. Cross sectioning and polishing was performed using Allied High Tech equipment using an aqueous polishing procedure developed by Allied High Tech for this application. The aqueous procedure may dissolve some compounds leaving voids visible in the cross sections.

3. Results

Fig. 2a shows the plot of specific mass change against time for the "in pack" and "out of pack" conditions. Also included for comparison are the results from the previously reported "no pack" study [21].

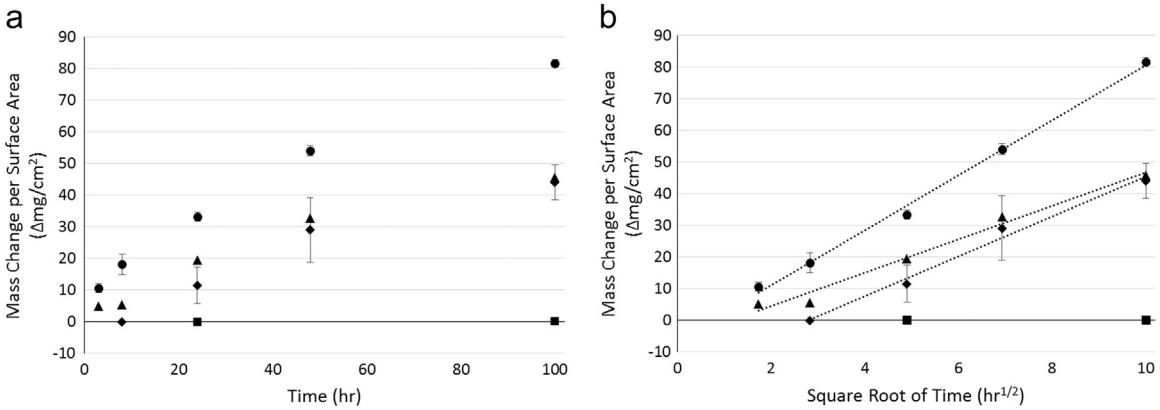

Fig. 2. The specific mass change plotted against a.) time and b.) square root of time for samples • in pack; ▲ out of pack; ◆ no pack from a previous study [21]; ■ reducing diffusion. Where present, the error bars represent a 95% confidence interval on the mean.

Fig. 2b shows this same data on transformed axes to display the fit with parabolic kinetics. This plot shows that the "in pack" and "out of pack" data closely follows parabolic kinetics, even at the shortest time interval of 3 h. This indicates that surface corrosion layers formed from “in pack” and “out of pack” conditions establish themselves quickly. This is in contrast to the “no pack” case where it took approximately 8 h for parabolic kinetics to begin; a delay attributed to initial chloride formation before a silicide layer could be established [21]. The "in pack" error bars represent a 95% confidence interval. These error bars are fairly small compared to “no pack” error bars, indicating the samples were exposed to a very consistent atmosphere. There are no error bars on the "out of pack" data because there was only one "out of pack" sample per run. Fig. 2a and b also show the mass data for “in pack” samples that were only exposed to a reducing environment, not a H_2/STC environment. These runs were performed to measure the influence of silicon diffusion into iron at these temperatures. The reducing environment was required to prevent silicon or iron oxidation. The input for these runs was a 5% hydrogen, 95% argon gas mixture. While the pO_2 was not explicitly measured in these runs, it was low enough that there was no surface iron oxide or silicon oxide detected with EDS or XRD after exposure. As is shown in the plot, the influence of diffusion is minor as there is near-negligible mass change to the iron samples after 100 h at 600 °C. This result is consistent with previous diffusion studies [24].

Fig. 3 shows the plan view FEM micrographs for the "in pack" samples after various time intervals. These images show fairly consistent surface topography at the various time intervals. The main difference between time intervals seems to be the larger nodules at longer times. Fig. 4 shows the FEM micrographs for the "out of pack" samples. Similar to the “in pack” samples, the main result is that longer exposure times resulted in larger nodules on the surface. Comparing “in pack” to “out of pack” samples shows that “in pack” samples have consistently larger nodules for a consistent time exposure. EDS analysis showed surface compositions consistent with stoichiometric FeSi for all samples.

XRD patterns were collected for 2 Theta equaling 15–70°. The patterns between 40° and 50° are shown for "in pack" and "out of pack" samples in Fig. 5a and b respectively. The range of 40–50° was selected

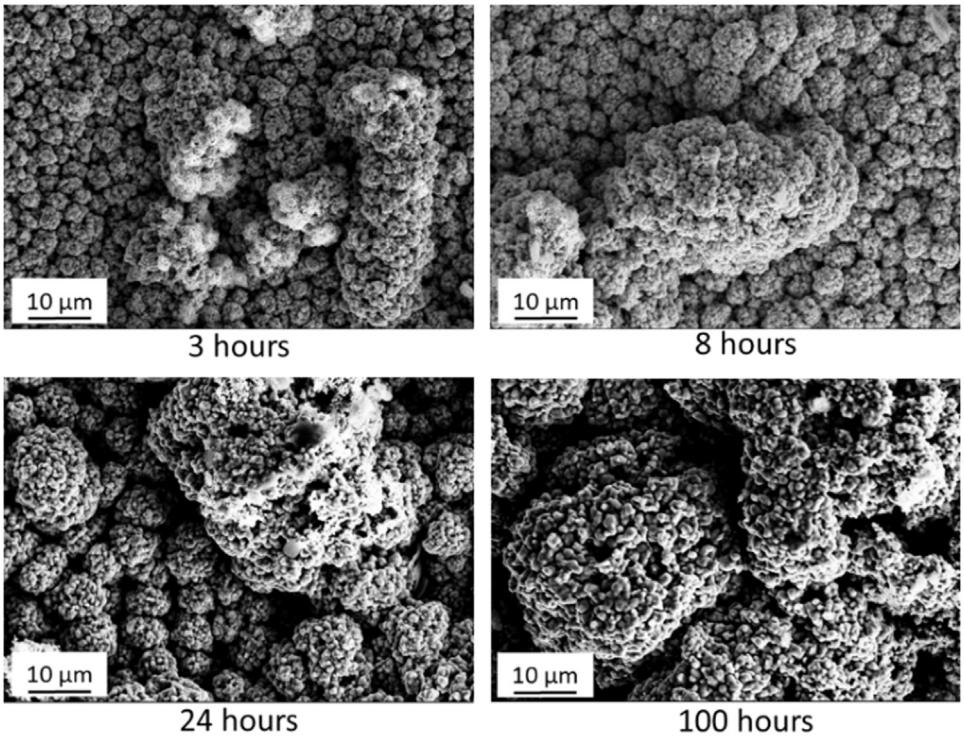

Fig. 3. Plan view FEM images of “in pack” samples exposed for a variety of times at 600 °C.

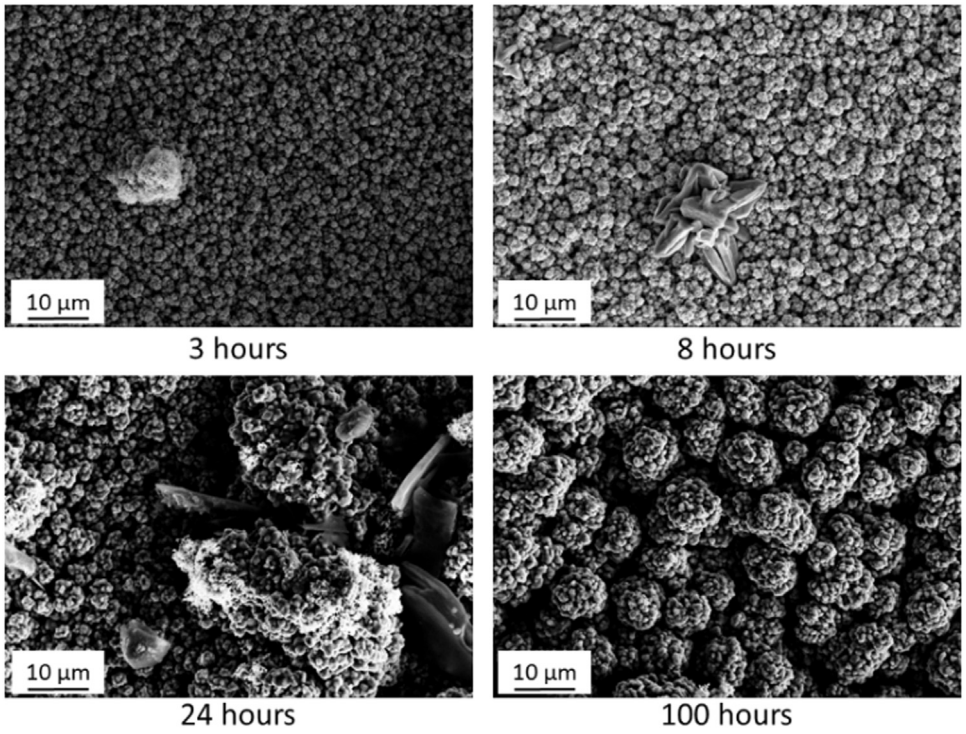

Fig. 4. Plan view FEM images of "out of pack" samples exposed for a variety of times at 600 °C.

because it encompassed all major peaks of interest [26–28]. It appears from these patterns that there was no detectable alpha (BCC) iron within the interaction volume of the XRD analysis for any of the exposed samples. This is significant because it implies that there is a relatively thick corrosion layer on the surface of the samples that covers any remaining pure iron in the middle. Fig. 5a shows that for "in pack" samples, primarily FeSi was detected after all time intervals. There was some Fe_3Si present, but it is relatively small compared to FeSi. Fig. 5b shows that for "out of pack" samples, there is primarily Fe_3Si after three hours, but that transitions to primarily FeSi at longer time intervals. After all time intervals, there was more FeSi on the "in pack" samples compared to the "out of pack" samples. This indicates a thicker FeSi layer on the "in pack" samples that more completely covers the Fe_3Si layer compared to "out of pack" samples.

Cross sectional analysis was able to confirm this claim. Fig. 6 shows the full width cross section of an "in pack" sample after 100 h of exposure at 600 °C. The EDS line scan shows an iron and silicon containing layer approximately 600–700 µm thick. The atomic concentrations are consistent with stoichiometric Fe_3Si that was detected with XRD. The interface between the unreacted iron and Fe_3Si region appears to be a gradual decrease in Si concentration rather than a step decrease. A higher magnification image of the edge of this sample is shown in Fig. 7. The EDS line scan associated with this image shows atomic concentrations consistent with a FeSi region approximately 150 µm thick on top of the Fe_3Si layer. Both the FeSi and Fe_3Si layers appear to be quite dense with only minor amounts of porosity. The surface of the sample (edge of the cross section) is very jagged with sharp peaks emerging from the bulk. Fig. 8 shows the full width cross section of an "out of pack" sample after 100 h at 600 °C. This sample has a similar structure to the "in pack" sample, but with a much thinner corrosion layer. The Fe_3Si layer in this sample was approximately 350 µm thick. Fig. 9 shows a higher magnification image of the same sample, and the FeSi layer in this sample appears to be only approximately 20 µm thick. The corrosion layer for this "out of pack" sample has slightly more porosity than the "in pack" sample, but it is still relatively dense.

Fig. 10 shows the cross section of an "in pack" iron sample exposed for 8 h. This image shows a similar transition from pure iron to stoichiometric Fe_3Si. It also appears to show a transition from Fe_3Si to FeSi. To confirm this, a higher magnification cross section is shown in

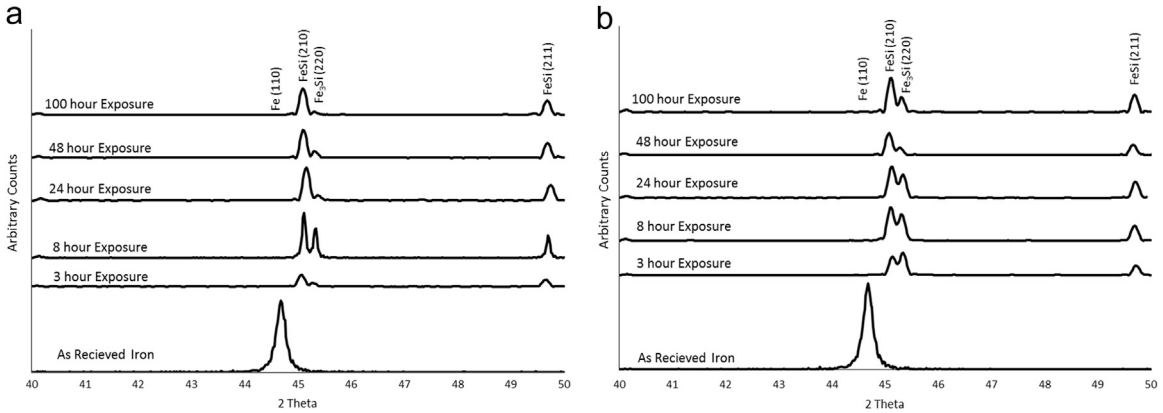

Fig. 5. XRD patterns of a.) "in pack" and b.) "out of pack" samples after a variety of times at 600 °C exposures. Peaks are labeled according to identification with Jade software [26–28].

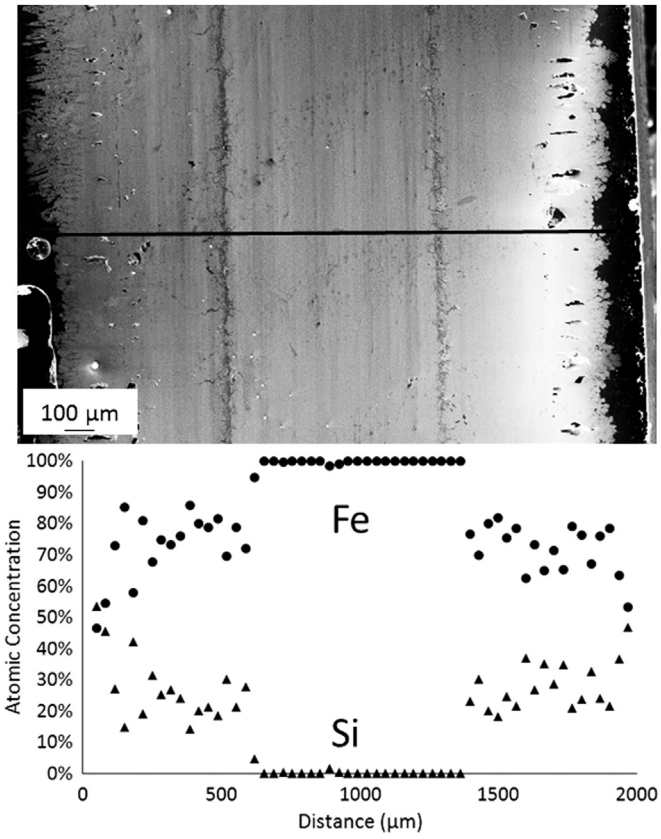

Fig. 6. Full width cross section and EDS line scan of "in pack" sample exposed for 100 h at 600 °C.

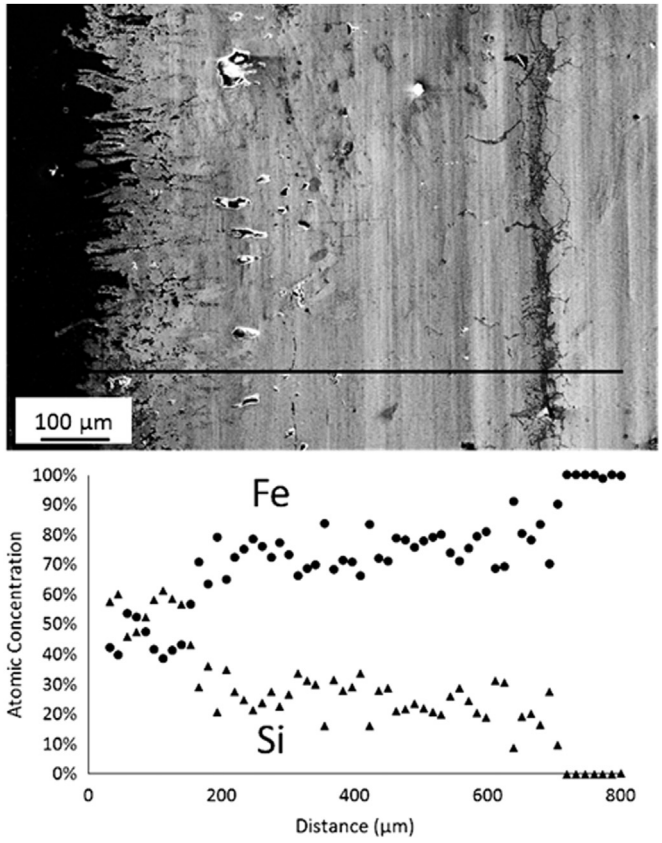

Fig. 7. High magnification image and EDS line scan of "in pack" sample exposed for 100 h at 600 °C.

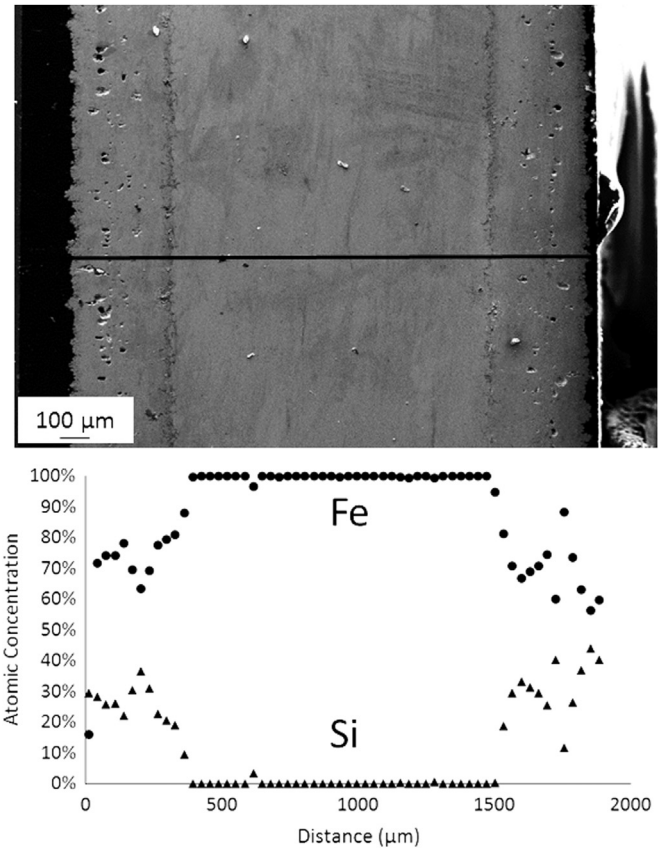

Fig. 8. Full width cross section and EDS line scan of "out of pack" sample exposed for 100 h at 600 °C.

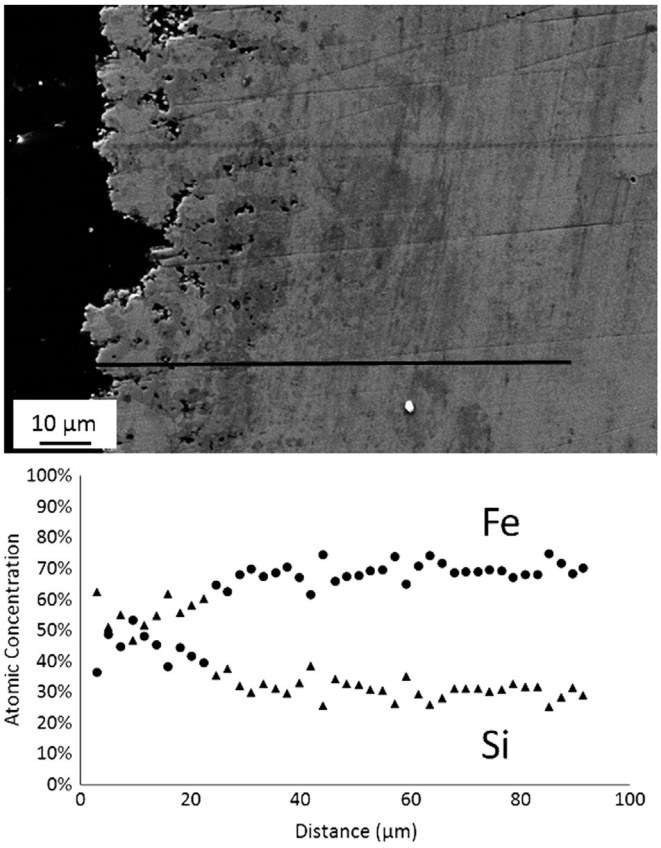

Fig. 9. High magnification image and EDS line scan of "out of pack" sample exposed for 100 h at 600 °C.

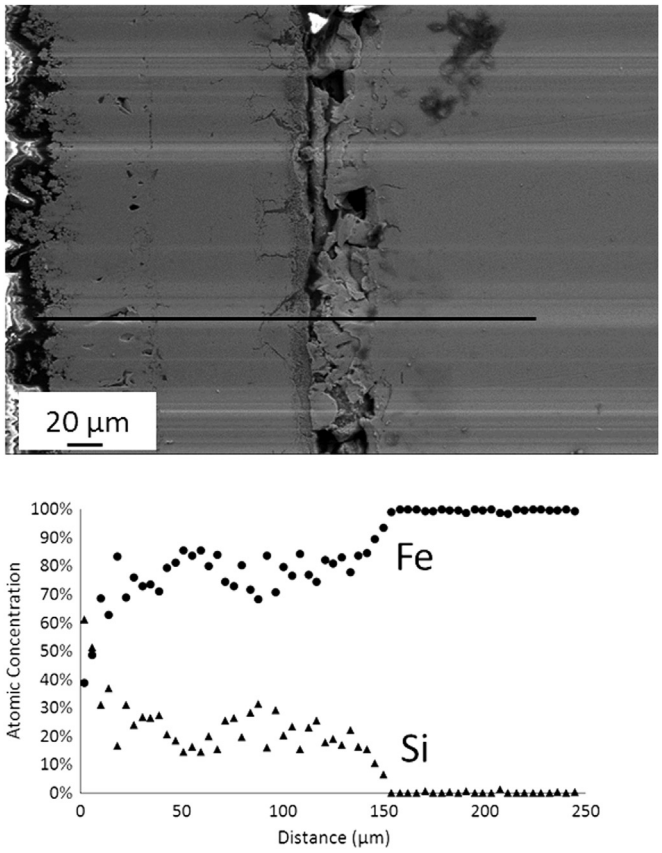

Fig. 10. FEM image and EDS line scan of "in pack" sample exposed for 8 h at 600 °C.

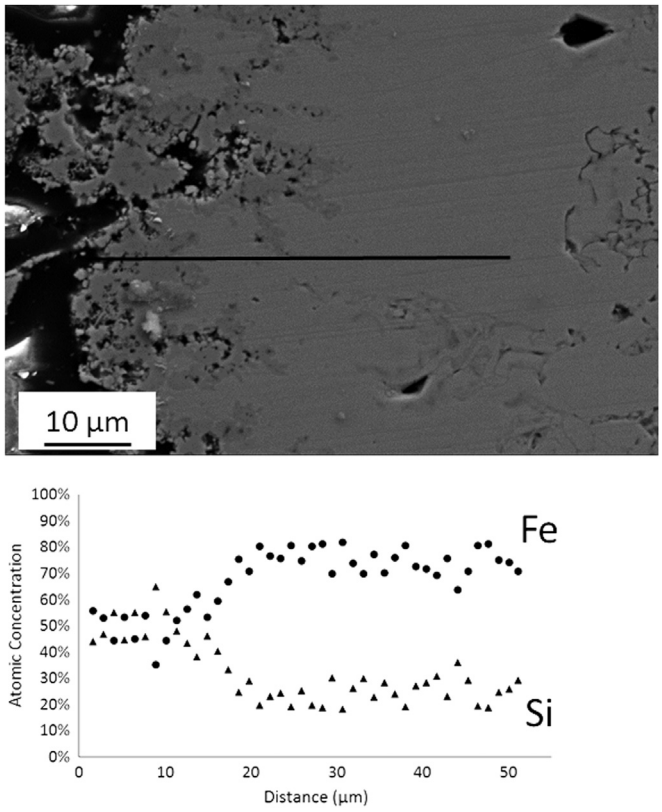

Fig. 11. High magnification image and EDS line scan of "in pack" sample exposed for 8 h at 600 °C.

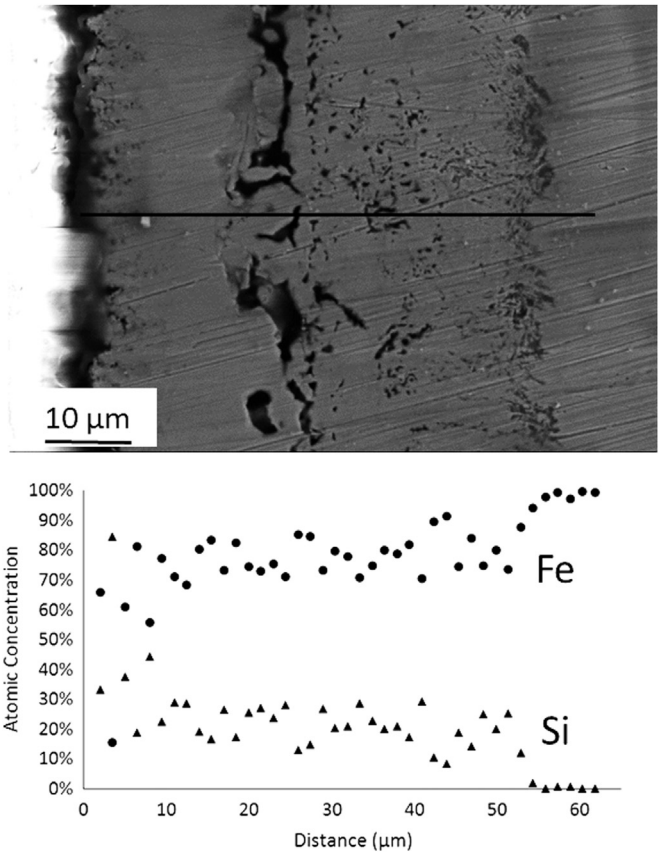

Fig. 12. High magnification image and EDS line scan of "out of pack" sample exposed for 8 h at 600 °C.

Fig. 11. This figure clearly shows a layer of stoichiometric FeSi followed by a layer of Fe_3Si. The FeSi layer is approximately 14 µm thick and the Fe_3Si layer is approximately 140 µm thick, which is significant for only 8 h of exposure. A comparable "out of pack" sample is shown in Fig. 12. This figure shows a much thinner Fe_3Si layer compared to the "in pack" sample, equaling only approximately 50 µm. A high magnification line scan of this sample revealed a FeSi layer approximately 8 µm thick, also much thinner than the comparable "in pack" sample. A comparison of Figs. 10 and 12 also reveals significantly more porosity in the "out of pack" sample, a trend also seen in the 100 h exposure.

4. Discussion

It is clear that embedding iron samples in metallurgical grade silicon increases the iron silicide layer thickness formed from an STC/H_2 input stream. However, it is likely that this increase is not due to significant solid diffusion of silicon into the iron. This is because the iron samples gained essentially zero mass and had no surface chemistry changes when they were exposed to a reducing environment while embedded in MG-Si. Therefore, it is likely that the MG-Si reacted with the chlorosilane gas at 600 °C to form a gas phase with a higher silicon activity. FactSage thermochemical software with FactPS 7.0 database was used to calculate chemical equilibrium for several cases to help explain the higher silicon activity [29]. The results are displayed in Table 1. The lower cutoff limit for all species was 1.0E−10 mol fraction. A fixed mole fraction of 0.74 H_2 and 0.26 STC was used to represent a tube furnace where reactants are constantly being added to the mixture. The first calculation allowed these reactants to reach equilibrium at 600 °C without additional silicon. This calculation revealed that many other species form at equilibrium including HCl, TCS, and DCS. This represents the "no pack" scenario reported previously in the literature. At equilibrium, this mixture has a silicon activity of 0.00184.

Table 1
Equilibrium gas composition calculated by FactSage for several cases relevant for chlorosilane corrosion.

Equilibrium Mole Fractions at 600 °C Room Temperature Input: Fixed 0.74 H_2/0.26 STC	**Additional Si**		
	None	1 mol Si	100 mol Si
H_2	7.11E–01	6.72E–01	6.72E–01
STC	2.50E–01	2.36E–01	2.36E–01
HCl	1.97E–02	4.06E–03	4.06E–03
TCS	1.94E–02	8.42E–02	8.42E–02
DCS	1.37E–04	2.74E–03	2.74E–03
$SiCl_3$	6.03E–05	2.62E–04	2.62E–04
$SiCl_2$	8.54E–07	1.70E–05	1.70E–05
SiH_3Cl	2.33E–07	2.14E–05	2.14E–05
SiH_4	1.79E–10	7.54E–08	7.54E–08
Si (s) Activity	1.84E–03	5.47E–01	5.47E–01

The next calculations included fixed silicon content to simulate the presence of MG-Si. At equilibrium, it does not matter how much silicon started in the system because it will all react with the flowing H_2 and STC. Comparing the equilibrium simulations with and without silicon indicates that the additional silicon has significant influence on the gas phase equilibrium. In the simulation with additional Si, there is significantly more TCS and DCS with less HCl compared to the simulation without additional Si. Also, the silicon activity for the simulation with additional Si is 0.547, over two orders of magnitude higher than the calculated Si activity without silicon (0.00184). This represents the gas environment experienced by the "in pack" samples in this study.

There was clear evidence for silicon consumption in the experiment to support the theory that silicon was added to the gas phase. FEM micrographs of the MG-Si before and after exposure are shown in Fig. 13. The as-received MG-Si contained granules approximately 100–400 μm in diameter that had relatively smooth edges. The MG-Si after exposure contained significantly smaller granules that were very rough. It also changed from a jet black color as received to a brown color after exposure, potentially due to the changes in surface morphology. The mass of the MG-Si was taken before and after exposure so that the amount of MG-Si consumed could be calculated; the result is shown in Fig. 14. This provides evidence of MG-Si reacting in to the gas phase and changing the gas phase composition as predicted. It is also possible that silicon in the quartz tube could react with the input gas stream and increase the silicon activity. This reaction would necessarily consume the quartz tube. The quartz tube was visually inspected between all runs, and there was never a visual indication that the quartz tube was being consumed by the gas stream, even after thousands of hours of exposure. Therefore, it was considered a minor effect. Future work could involve characterizing the exhaust stream to confirm the change in gas stream composition and complete the silicon mass balance. However, this task was not performed in this series of experiments.

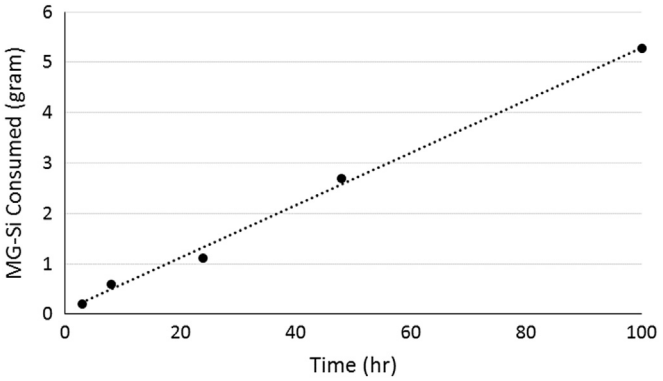

Fig. 14. Plot of MG-Si consumed per run time as measured by weighing the MG-Si before and after exposure. The calculated trend line was (MG-Si consumed (gram)) =0.0522* (Time (h))+0.0692 with an r-squared value of 0.996.

Higher silicon activities in the gas phase will correspond with higher silicon activities in the condensed phase. A predominance diagram that relates the iron based condensed phase with silicon and HCl activity has already been reported in the literature [21]. A higher silicon activity corresponds with a more silicon-rich iron silicide. Also, the predominance diagram predicts that a sufficiently high silicon

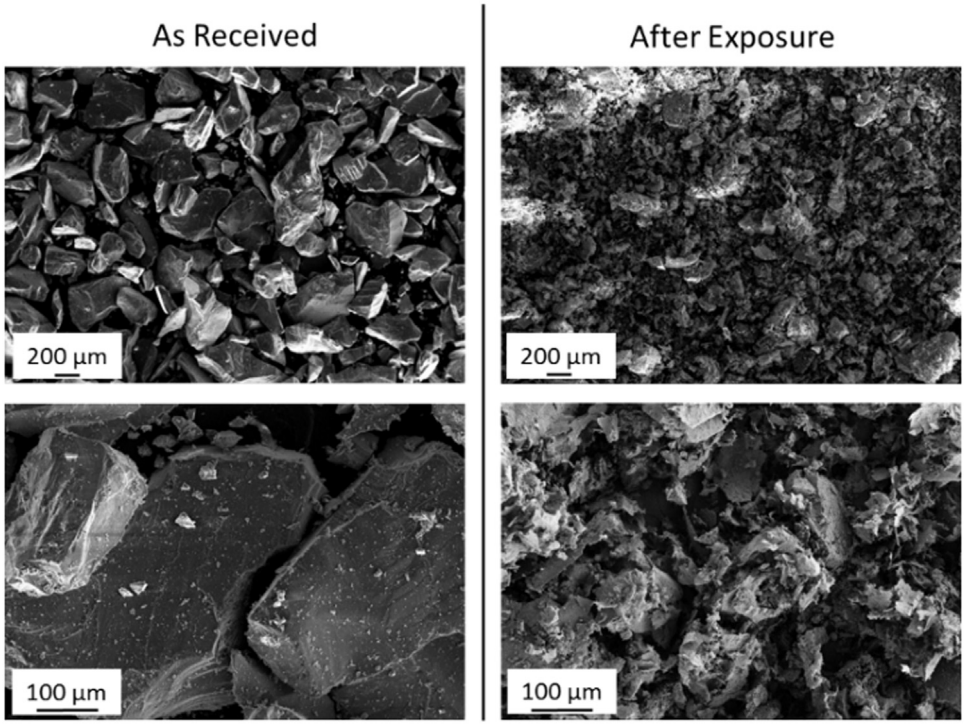

Fig. 13. FEM images of MG-Si as received and after 100 h exposure at 600 °C.

activity will prevent any iron chlorides from forming. Iron chlorides are volatile at 600 °C and are often to blame for porosity in corrosion layers [12,13,30]. Therefore, the thicker silicon-rich silicide layer and lack of porosity in the "in pack" samples compared to the "no pack" samples are likely due to increased silicon activity. The higher silicon activity also translates to the "out of pack" samples. The "out of pack" case is much more difficult to model thermodynamically. However, some inferences can be made based on the experimental results. The increased porosity and thinner FeSi layers of the "out of pack" samples compared to the "in pack" samples indicates a lower silicon activity for the "out of pack" samples. However, comparison to previously reported "no pack" samples indicates that the silicon activity in the "out of pack" case is higher than "no pack" [21]. This is likely due to the gas environment becoming more silicon rich as it flows over the packed bed of silicon, and the gas retaining that silicon as it exposes the "out of pack" samples.

This higher silicon activity has both helpful and harmful effects from a corrosion standpoint. The fact that it decreases or prevents iron chloride formation is helpful because the formation of volatile chlorides consumes the base metal and may lead to decreased metal thickness. However, the formation of silicon-rich iron silicides does not seem to be fully protective. The parabolic kinetics illustrated by the mass data is evident, but the cross sectional analysis shows that a significant amount of base iron has been converted to Fe_3Si or FeSi; both of which have different physical and chemical properties than pure iron.

5. Conclusions

This study investigates the chlorosilane corrosion behavior of pure iron and the influence of a packed bed of silicon at various time intervals and 600 °C. It was discovered that stratified surface layers of FeSi and Fe_3Si form very quickly in these conditions, and parabolic kinetics are present after just 3 h of exposure. FEM, EDS, and XRD were employed to confirm the presence of FeSi and Fe_3Si and their location relative to the base metal. The corrosion layers of "in pack" samples were significantly thicker than "out of pack" samples, likely due to the higher silicon activity in the pack. Additionally, there was less evidence of chloride formation on the "in pack" samples as seen by the lack of porosity. Comparison to previously reported predominance diagrams show that the lack of chloride formation is also likely from the increased silicon activity.

Thermochemical modeling was used to show the effect of MG-Si on the equilibrium composition of an input stream of STC and H_2. This modeling revealed an equilibrium silicon activity two orders of magnitude higher for the "in pack" case compared to "no pack". This increased gas phase silicon activity is due to solid silicon consumption, a claim confirmed by weighing and imaging the packed bed of MG-Si before and after exposure. Additionally, the implications of a higher silicon activity and the corrosion layers formed because of it were discussed. The results of this study show the importance of replicating a chlorosilane environment as precisely as possible to get appropriate corrosion data.

Acknowledgements

We would like to acknowledge the Montana State University College of Engineering for providing funding for this project. Additionally, we would like to acknowledge Montana State University's Imaging and Chemical Analysis Laboratory (ICAL) for their assistance with surface analysis.

References

[1] W.M. Ingle, M.S. Peffley, Kinetics of the hydrogenation of silicon tetrachloride, J. Electrochem. Soc. 132 (1985) 1236–1240.
[2] T.I. Kamins, Deformation occurring during the deposition of polycrystalline-silicon films, J. Electrochem. Soc. 121 (1974) 681–684.
[3] S.F. Nitodas, S.V. Sotirchos, Development and validation of a mathematical model for the chemical vapor deposition of silica from mixtures of chlorosilanes, carbon dioxide, and hydrogen, J. Electrochem. Soc. 149 (2002) C120–C129.
[4] T.O. Sedgwick, Analysis of the hydrogen reduction of silicon tetrachloride process on the basis of a quasi-equilibrium model, J. Electrochem. Soc. 111 (1964) 1381–1383.
[5] B. Hazeltine, Chad Fero, Wenjun Qin, Advancements in the commercial production of polysilicon, 2010.
[6] D.M. Powell, R. Fu, K. Horowitz, P.A. Basore, M. Woodhouse, T. Buonassisi, The capital intensity of photovoltaics manufacturing: barrier to scale and opportunity for innovation, Energy Environ. Sci. 8 (2015) 3395–3408.
[7] J.Y.P. Mui, Corrosion mechanism of metals and alloys in the silicon-hydrogen-chlorosilane system at 500 °C, Corrosion 41 (1985) 63–69.
[8] P. Li, T. Wang, Thermodynamic analysis of manufacturing polysilicon from $SiHCl_3$, $SiCl_4$ and H_2, Chin. J. Chem. Eng. 23 (2015) 681–688.
[9] J.Y. Lee, W.H. Lee, Y.-K. Park, H.Y. Kim, N.Y. Kang, K.B. Yoon, W.C. Choi, O.B. Yang, Catalytic conversion of silicon tetrachloride to trichlorosilane for a poly-Si process, Sol. Energy Mater. Sol. Cells 105 (2012) 142–147.
[10] Y. Ihara, H. Ohgame, K. Sakiyama, K. Hashimoto, The corrosion behaviour of iron in hydrogen chloride gas and gas mixtures of hydrogen chloride and oxygen at high temperatures, Corros. Sci. 21 (1981) 805–817.
[11] F.M. d'Heurle, P. Gas, Kinetics of formation of silicides: a review, J. Mater. Res. 1 (1986) 205–221.
[12] P. Daniel, R. Rapp, Halogen Corrosion of Metals, in: M. Fontana, R. Staehle (Eds.), Advances in Corrosion Science and Technology, Springer, US, 1976, pp. 55–172.
[13] P. Roberge, Handbook of Corrosion Engineering, Mcgraw-hill, 1999 ISBN number 9780070765160.
[14] M. Rebhan, R. Meier, A. Plagge, M. Rohwerder, M. Stratmann, High temperature chemical vapor deposition of silicon on Fe(100), Appl. Surf. Sci. 178 (2001) 194–200.
[15] M. Rebhan, M. Rohwerder, M. Stratmann, CVD of silicon and silicides on iron, Appl. Surf. Sci. 140 (1999) 99–105.
[16] C. Klam, J. Millet, H. Mazille, J. Gras, Chemical vapour deposition of silicon onto iron: influence of silicon vapour phase source on the composition and nature of the coating, J. Mater. Sci. 26 (1991) 4945–4952.
[17] J. Acker, K. Bohmhammel, Reactivity of intermetallic compounds: a solid state approach to direct reactions of silicon, J. Phys. Chem. B 106 (2002) 5105–5117.
[18] J. Acker, K. Bohmhammel, Compensation effect in trichlorosilane synthesis, J. Organomet. Chem. 686 (2003) 151–157.
[19] J. Acker, I. Röver, R. Otto, G. Roewer, K. Bohmhammel, Formation of transition metal silicides by solid–gas reactions: thermodynamic and kinetic considerations, Solid State Ion. 141–142 (2001) 583–591.
[20] J. Aller, K. Ellingwood, N. Jacobson, P. Gannon, High temperature chlorosilane corrosion of AISI 316L, J. Electrochem. Soc. 163 (2016) C452–C458.
[21] J. Aller, R. Mason, K. Walls, G. Tatar, N. Jacobson, P. Gannon, High-temperature (550–700 °C) chlorosilane interactions with iron, J. Electrochem. Soc. 163 (2016) C666–C674.
[22] J.L. Aller, K. Ellingwood, B. Clark, P.E. Gannon, The time and temperature dependence of AISI 316L corrosion in chlorosilane environments, ECS Trans. 66 (2015) 41–51.
[23] J.L. Aller, P. White, J. Gum, B. Clark, P.E. Gannon, High-temperature corrosion of AISI 316L in chlorosilane environments at 550 °C, ECS Trans. 64 (2015) 161–171.
[24] N.R. Baldwin, D.G. Ivey, Iron silicide formation in bulk iron-silicon diffusion couples, J. Phase Equilibria 16 (1995) 300–307.
[25] Y. Zhang, D.G. Ivey, Fe_3Si formation in Fe–Si diffusion couples, J. Mater. Sci. 33 (1998) 3131–3135.
[26] E.A. Owen, E.L. Yates, XLI, Precision measurements of crystal parameters, Lond. Edinb. Dublin Philos. Mag. J. Sci. 15 (1933) 472–488.
[27] F.A.B. Sidorenko, A.N. Shubina, T.S. Skripova, A. Ye, L.P. Zelenin, Magnetic susceptibility of solid solutions of the monosilicides FeSi–CoSi and FeSi–NiSi, Phys. Met. Metallogr. 28 (1969) 91–96.
[28] J. Waliszewski, L. Dobrzyński, A. Malinowski, D. Satuła, K. Szymański, W. Prandl, T. Brückel, O. Schärpf, Magnetic moment distribution in $Fe_{3-x}Cr_xSi$ alloys, J. Magn. Magn. Mater. 132 (1994) 349–358.
[29] C.W. Bale, P. Chartrand, S.A. Degterov, G. Eriksson, K. Hack, R. Ben Mahfoud, J. Melançon, A.D. Pelton, S. Petersen, FactSage thermochemical software and databases, Calphad 26 (2002) 189–228.
[30] N.S. Jacobson, Reaction of iron with hydrogen chloride-oxygen mixtures at 550 °C, Oxid. Met. 26 (1986) 157–169.